Analysis of groundwater flow and stream depletion in L-shaped fluvial aquifers

Chao-Chih Lin[1], Ya-Chi Chang[2] and Hund-Der Yeh[1]

[1]Institute of Environmental Engineering, National Chiao Tung University, Hsinchu, Taiwan
5 [2]Taiwan Typhoon and Flood Research Institute, National Applied Research Laboratories, Taipei, Taiwan

Correspondence to: Hund-Der Yeh (hdyeh@mail.nctu.edu.tw)

Abstract. Understanding the head distribution in aquifers is crucial for the evaluation of groundwater resources. This article develops a model for describing flow induced by pumping in an L-shaped fluvial aquifer bounded by impermeable bedrocks and two nearly fully penetrating streams. A similar scenario for numerical studies was reported in Kihm et al. (2007). The

10 water level of the streams is assumed to be linearly varying with distance. The aquifer is divided into two sub-regions and the continuity conditions of hydraulic head and flux are imposed at the interface of the sub-regions. The steady-state solution describing the head distribution for the model without pumping is first developed by the method of separation of variables. The transient solution for the head distribution induced by pumping is then derived based on the steady-state solution as initial condition and the methods of finite Fourier transform and Laplace transform. Moreover, the solution for stream depletion rate

15 (*SDR*) from each of the two streams is also developed based on the head solution and Darcy's law. Both head and *SDR* solutions in real time domain are obtained by a numerical inversion scheme called the Stehfest algorithm. The software MODFLOW is chosen to compare with the proposed head solution for the L-shaped aquifer. The steady-state and transient head distributions within the L-shaped aquifer predicted by the present solution are compared with the numerical simulations and measurement data presented in Kihm et al. (2007).

20 **1 Introduction**

Groundwater is an important water resource for agricultural, municipal and industrial uses. The planning and management of water resources through the investigation of groundwater flow is one of the major tasks for practicing engineers. The aquifer type and shape are important factors influencing the groundwater flow. Many studies have been devoted to the development of analytical models for describing flow in finite aquifers with a rectangular boundary (e.g., Chan et al., 1976; Chan et al.,

25 1977; Daly and Morel-Seytoux, 1981; Latinopoulos, 1982; Corapcioglu et al., 1983; Latinopoulos, 1984, 1985; Lu et al., 2015), a wedge-shaped boundary (Chan et al., 1978; Falade, 1982; Holzbecher, 2005; Yeh et al., 2008; Chen et al., 2009; Samani and Zarei-Doudeji, 2012; Samani and Sedghi, 2015; Kacimov et al. 2016), a triangle boundary (Asadi-Aghbolaghi et al., 2010) a trapezoidal-shaped boundary (Mahdavi and Seyyedian, 2014), or a meniscus-shaped domain (Kacimov et al. 2017). So far, the case of re-entrant angle (L-shaped) boundaries has been treated analytically in different fields such as torsion of elastic bars

(Kantorovich and Krylov, 1958), head fluctuation problems for tidal aquifers (Sun, 1997; Li and Jiao, 2002), and heat conduction in plates (Mackowski, 2011). However, none of the cited papers deals with pumping or stream depletion problems. Many studies focused on the development of numerical approaches to model groundwater flow in an aquifer with irregular domain and various types of boundary conditions. The rapid increase of the computing power of PC enables the numerical

5   models to handle the groundwater flow problems with complicated geometric shapes and/or heterogeneous aquifer. Numerical methods such as finite element methods (FEMs) and finite difference methods (FDMs) are very commonly used in engineering simulations or analyses. For the application of FEMs, Taigbenu (2003) solved the transient flow problems based on the Green element method for multi-aquifer systems with arbitrary geometries. Kihm et al. (2007) used a general multidimensional hydrogeomechanical Galerkin FEM to analyze three-dimensional (3D) problems of saturated-unsaturated flow and land

10   displacement induced by pumping in a fluvial aquifer in Yongpoong 2 Agriculture District, Gyeonggi-Do, Korea. The domain of the aquifer is in L shape and bounded by streams and impermeable bedrock. Their mathematical model was developed with considering the unsaturated flow and solid skeleton deformation to a set of four coupled nonlinear equations in terms of one head variable and three displacement variables. The Galerkin FEM was employed to simulate the steady-state spatial distribution of hydraulic head before aquifer pumping and then the distributions of hydraulic head and land displacement vector

15   after one-year pumping. Their simulation results were compared and validated with the field measurements of hydraulic head and vertical displacement in the transient case. However, it was a lot of work to solve the simultaneous nonlinear equation and might difficult be applied because it took a lot of calculation time and resources for long-term simulations.

The FDMs have been widely utilized in the groundwater problems too. Mohanty et al. (2013) evaluated the performances of the finite difference groundwater model MODFLOW and the computational model artificial neural network (ANN) in the

20   simulation of groundwater level in an alluvial aquifer system. They compared the results with field observed data and found that the numerical model is suitable for long-term predictions, whereas the ANN model is appropriate for short-term applications. Serrano (2013) illustrated the use of Adomian's decomposition method to solve a regional groundwater flow problem in an unconfined aquifer bounded by the main stream on one side, two tributaries on two sides, and an impervious boundary on the other side. He demonstrated an application to an aquifer bounded by four streams with a deep excavation

25   inside where the head was kept constant. Jafari et al. (2016) incorporated Terzaghi's theory of one-dimensional consolidation with MODFLOW to evaluate groundwater flow and land subsidence due to heavy pumping in a basin aquifer in Iran. So far, many computer codes developed based on either FDMs (e.g., FTWORK and MODFLOW), FEMs (e.g., AQUIFEM-N, BEMLAP, FEMWATER, and SUTRA) or boundary element methods (e.g., BEMLAP) had been employed to simulate a variety of groundwater flow problems (Loudyi et al., 2007).

30   On the other hand, analytical solutions are convenient and powerful tools to explore the physical insight of groundwater flow systems. The head solution is capable of predicting the spatiotemporal distribution of the drawdown at any location within the simulation time and the stream depletion rate (*SDR*) solution can estimate the stream filtration rate at any instance at a specific location in the groundwater flow system. Thus, the development of analytical models for describing the groundwater flow in a heterogeneous aquifer with irregular outer boundaries and subject to various types of boundary condition is of practical use

from an engineering viewpoint. Kuo et al. (1994) applied the image well theory and Theis' equation to estimate transient drawdown in an aquifer with irregularly shaped boundaries. The aquifer is an oil reservoir bounded by three tortuous faults. However, the number of the image wells should be largely increased if the aquifer boundary is asymmetric and rather irregular. Insufficient number of the image wells might result in poor results or even divergence (Matthews et al., 1954). Read and

5 Volker (1993) presented analytical solutions for steady seepage through hillsides with arbitrary flow boundaries. They used the least squares method to estimate the coefficients in a series expansion of the Laplace equation. Li et al. (1996) extended the results of Read and Volker (1993) in solving the two-dimensional (2D) groundwater flow in porous media governed by Laplace's equation involving arbitrary boundary conditions. The solution procedure was obtained by means of an infinite series of orthonomal functions. Additionally, they also introduced a method, called image-recharge method, to establish the

10 recurrence relationship of the series coefficients. Patel and Serrano (2011) solved nonlinear boundary value problems of multidimensional equations by Adomian's method of decomposition for groundwater flow in irregularly shaped aquifer domains. Mahdavi and Seyyedian (2014) developed a semi-analytical solution for hydraulic head distribution in trapezoidal-shaped aquifers in response to diffusive recharge of constant rate. The aquifer was surrounded by four fully penetrating and constant-head streams. Kacimov et al. (2016) used the Strack-Chernyshov model to investigate the unconfined groundwater

15 flows in a wedge-shaped promontories with accretion along the water table and outflow from a groundwater mound into draining rays. Huang et al. (2016) presented 3D analytical solutions for hydraulic head distributions and *SDR*s induced by a radial collector well in a rectangular confined or unconfined aquifer bounded by two parallel streams and no-flow boundaries. Currently, the distribution of groundwater flow velocity in a circular meniscus aquifer was investigated analytically by theory of holomorphic functions and numerically by FEM (Kacimov et al., 2016).

20 Groundwater pumping near a stream in a fluvial aquifer may cause the dispute of stream water right, impact of aquatic ecosystem in stream, as well as water allocation or management problems for agriculture, industry, and municipality. The impacts of groundwater extraction by wells should therefore be thoroughly investigated before pumping. Theoretically, numerical methods, such as FEM are good tools to simulate groundwater flow in irregular-shaped aquifer such as the approximately L-shaped aquifer in Kihm et al. (2007). However, they are generally time consuming and demanding of

25 computing power (Younger, 2007), and it is necessary to re-generate the mesh of problem domain for different size of L-shaped aquifers. The analytical solution can be easily applied for different size of L-shaped aquifer with similar boundaries and properties by replacing the length or width of the solution. Thus, an analytical solution is proposed in this study to evaluate the spatiotemporal distribution of the drawdown at any location in the L-shaped aquifer. This paper develops a 2D mathematical model for describing the groundwater flow in an approximately L-shaped fluvial aquifer which is very close to

30 the case of numerical simulations reported in Kihm et al. (2007). The aquifer is divided into two rectangular sub-regions. The aquifer in each sub-region is assumed to be homogeneous but anisotropic in the horizontal plane with principal direction aligned with the borderline of the rectangular sub-regions. Three types of boundary conditions including constant-head, linearly varying head, and no-flow are adopted to reflect the physical reality at the outer boundaries of the problem domain. A steady-state solution is first developed to represent the hydraulic head distribution within the aquifer before pumping. The

transient head solution of the model is then obtained using the Fourier finite sine and cosine transforms and the Laplace transform. The Stehfest algorithm is then taken to invert the Laplace-domain solution for the time-domain results. The software MODFLOW for the simulation of the 3D groundwater flow is used to evaluate the present head solutions. The *SDR* solution is also derived based on the head solution and Darcy's law and then used to evaluate the contribution of filtration water from each of two streams toward the pumping well.

2 Methodology

Figure 1 shows a fluvial plain located in Yongpoong 2 Agriculture District, Gyeonggi-Do, Korea whose characteristics are reported in Kihm et al. (2007). The west side of the plain is a mountainous area, where impermeable bedrock outcrops, and the Poonggye stream flows along the east side from the southwest corner toward the northeast corner. A tributary of Poonggye stream, entering the stream with nearly a right angle, is on the north side of the plain. The Poonggye stream and its tributary are perennial streams and almost fully penetrate the fluvial aquifer system (Kihm et al., 2007). The width of Poonggye stream is about 15m as reported in Rhms (2013).

2.1 Conceptual Model

The aquifer in the district is formed by fluvial deposits with a total thickness of 6 m, and consists of a clay loam aquitard with a thickness of about 2.5 m underlain by a loamy sand layer with a thickness of about 3.5 m (Kihm et al., 2007). In order to develop an analytical model for solving the groundwater flow, the domain of the aquifer in this study is approximated to be L-shaped, as delineated in Figure 2. Notice that in Figure 1 the solid line denotes the outer boundary of the L-shaped aquifer in this study while the dashed line represents the simulation area in the work of Kihm et al. (2007). The origin of the coordinates in Figure 2 is at the lower left corner of point A, which is at the intersection of boundary AB (i.e., a part of Poonggye stream) and boundary AG. The boundaries of the aquifer domain along EF and FG are impermeable bedrocks and thus regarded as impermeable boundaries. The annual average heads above the bottom of the aquifer are respectively identified as 5.18 m, 4.06 m and 5.29 m at points A, B, and D (Kihm et al., 2007). The hydraulic heads along AG and DE are assumed equal to their average head values done by Kihm et al. (2007). In other words, the boundaries along AG and DE are assumed under the constant-head condition in our mathematical model. Physically, they do not coincide with streams and therefore do not contribute to *SDR* as calculated in Sect. 2.5 Stream depletion rate. The boundaries AB and BD are designated to represent the Poonggye stream and its tributary, respectively. Kihm et al. (2007) fixed the hydraulic heads of Poonggye stream and its tributary at annual average water stages in their numerical simulations. Thus, this study considers that the stream has a perfect hydraulic connection with the aquifer and the stream stage varies linearly with distance. The average stream flow rate of the Poonggye stream with its tributary is about 100 m^3/s as reported by Rhms (2013, p. 90). Pumping wells in the conceptual model are assumed to fully penetrate the aquifer near the perennial stream AB as mentioned in Kihm et al. (2007), and therefore the hydraulic gradient in vertical direction is neglected. Todd and Mays (2005, p. 232) noticed that the discharge rates in a

shallow well may range up to 500 m³/day (0.01 m³/s) and the suction lifts should be less than 7 m for efficient and continuous service. Hence, the effect of pumping in a shallow well on the water table of nearby stream is generally negligible. The annual average depth from the ground surface to the water table is 1.26 m with a spatial variation from 0.57 m to 1.95 m in accordance with the average water stages in the streams AB and BD (Kihm et al., 2007). The depth for the aquifer system before pumping was estimated under the hydrostatic equilibrium condition and with considering the effect of net annual average rainfall.

2.2 Mathematical model

As shown in Figure 2, the aquifer is divided into two sub-regions named as regions 1 and 2 and variables $\phi_1(x, y, t)$ and $\phi_2(x, y, t)$ are their corresponding hydraulic heads. Consider that there are totally M pumping wells in region 1 and N pumping wells in region 2, and all the pumping wells fully penetrate the aquifer. The coordinates of kth well in region 1 and lth well in region 2 are denoted as (x_{1k}, y_{1k}) and (x_{2l}, y_{2l}), respectively, and the pumping rate per unit thickness at kth well is represented by Q_{1k} $[L^2/T]$ and that at lth well is Q_{2l} $[L^2/T]$. The governing equations describing 2D hydraulic head distributions in region 1 and region 2 are respectively expressed as

$$K_{x1}\frac{\partial^2 \phi_1}{\partial x^2} + K_{y1}\frac{\partial^2 \phi_1}{\partial y^2} = S_{s1}\frac{\partial \phi_1}{\partial t} - \sum_{k=1}^{M} Q_{1k}\delta(x - x_{1k})\delta(y - y_{1k})$$

$$0 \leq x \leq l_1, 0 \leq y \leq d_1 \tag{1}$$

$$K_{x2}\frac{\partial^2 \phi_2}{\partial x^2} + K_{y2}\frac{\partial^2 \phi_2}{\partial y^2} = S_{s2}\frac{\partial \phi_2}{\partial t} - \sum_{l=1}^{N} Q_{2l}\delta(x - x_{2l})\delta(y - y_{2l})$$

$$l_2 \leq x \leq l_1, d_1 \leq y \leq d_2 \tag{2}$$

where $K_x[L/T]$ and $K_y[L/T]$ are respectively the hydraulic conductivities in x- and y-direction, and S_s $[L^{-1}]$ is the specific storage. The symbol δ represents one dimensional (1D) Dirac's delta function $[1/T]$.

The boundary conditions for region 1 are expressed as:

$$\phi_1(0, y) = h_1 \text{ for AG} \tag{3}$$

$$\phi_1(l_1, y) = h_3 + \frac{h_2 - h_3}{b_2}y \text{ for BC} \tag{4}$$

$$\phi_1(x, 0) = h_1 + \frac{h_3 - h_1}{l_1}x \text{ for AB} \tag{5}$$

$$\frac{\partial \phi_1}{\partial y}(x, d_1) = 0 \text{ for FG} \tag{6}$$

Similarly, the boundary conditions for flow in region 2 are

$$\frac{\partial \phi_2}{\partial x}(l_2, y) = 0 \text{ for EF} \tag{7}$$

$$\phi_2(l_1, y) = h_3 + \frac{h_2 - h_3}{b_2} y \text{ for CD} \tag{8}$$

$$\phi_2(x, d_2) = h_2 \text{ for DE} \tag{9}$$

The continuity requirements of hydraulic head and flux along the interface CF are respectively

$$\phi_1(x, d_1) = \phi_2(x, d_1) \tag{10}$$

and

$$K_{y1} \frac{\partial \phi_1}{\partial y}\bigg|_{y=d_1} = K_{y2} \frac{\partial \phi_2}{\partial y}\bigg|_{y=d_1} \tag{11}$$

In order to express the solution in dimensionless form, the following dimensionless variables or parameters are introduced: $\phi_1^* = (\phi_1 - h_1)/h_1$, $\phi_2^* = (\phi_2 - h_1)/h_2$, $t^* = K_{y1}t/S_{s1}d_2^2$, $\kappa_1 = K_{x1}/K_{y1}$, $\kappa_2 = K_{x2}/K_{y2}$, $x^* = x/l_1$, $y^* = y/d_2$, $d_1^* = d_1/d_2$, $l_2^* = l_2/l_1$, $Q_{1k}^* = d_2^2 Q_{1k}/K_{y1}h_1$ and $Q_{2l}^* = d_2^2 Q_{2l}/K_{y2}h_2$ where ϕ_1^* and ϕ_2^* stand for the dimensionless hydraulic heads in regions 1 and 2, respectively; t^* refers to the dimensionless time during the test; κ_1 and κ_2 represent the anisotropic ratio of hydraulic conductivity in regions 1 and 2, respectively; x^* and y^* denote the dimensionless coordinates.

2.3 Steady-state solution for hydraulic head distribution

In order to compare the steady-state simulations of Kihm et al. (2007) without pumping, the steady-state solution for the hydraulic head distribution in the L-shaped aquifer is developed. Detailed derivation for the analytical solutions in steady state for regions 1 and 2 is given in Appendix A, and the results are expressed respectively as (Chu et al., 2012)

$$\phi_1^*(x^*, y^*) = \sum_{m=1}^{\infty} \Delta_1 [C_{1m} E_1(m, y^*) + F_1(m, y^*)] \sin(\lambda_m x^*) \tag{12}$$

and

$$\phi_2^*(x^*, y^*) = \sum_{n=1}^{\infty} \Delta_2 [D_{2n} E_2(n, y^*) + F_2(n, y^*)] \cos[\alpha_n(x^* - l_2^*)] \tag{13}$$

with

$$E_1(m, y^*) = \frac{e^{\Omega_{1m} y^*} - e^{-\Omega_{1m} y^*}}{e^{\Omega_{1m} b_1^*} - e^{-\Omega_{1m} b_1^*}} \tag{14}$$

$$F_1(m, y^*) = \frac{1}{\lambda_m} (-1)^{m+1} (h_{31}^* + h_{23}^* y^*) \tag{15}$$

$$E_2(n, y^*) = e^{-\Omega_{2n} y^*} - e^{\Omega_{2n}(y^* - 2)} \tag{16}$$

$$F_2(n, y^*) = \frac{(-1)^{n-1}}{\alpha_n} (H_{31}^* + H_{23}^* y^*) \tag{17}$$

where the symbols and dimensionless variables Δ_1, Δ_2, λ_m, α_n, Ω_{1m}, Ω_{2n}, h_{31}^*, h_{23}^*, H_{23}^* and H_{31}^* are defined in Table 1. The coefficients C_{1m} and D_{2n} can be determined simultaneously by the continuity conditions of hydraulic head and flux along the interface CF. The results are denoted as follows:

$$C_{1m} = \frac{\Delta_2}{2}\frac{K_{y2}}{K_{y1}}\frac{h_2}{h_1}\sum_{n=1}^{\infty}\left[D_{2n}\frac{E_2{'}(n,y^*)}{E_1{'}(m,y^*)}\Big|_{y^*=b_1^*} + \frac{F_2{'}(n,y^*)}{E_1{'}(m,y^*)}\Big|_{y^*=b_1^*}\right]G_1(m,n) - \frac{F_1{'}(m,y^*)}{E_1{'}(m,y^*)}\Big|_{y^*=b_1^*} \tag{18}$$

5   and

$$D_{2n} = \frac{1}{\Delta_2}\frac{h_1}{h_2}\sum_{m=0}^{\infty}\left[C_{1m}\frac{E_1(m,d_1^*)}{E_2(n,d_1^*)} + \frac{F_1(m,d_1^*)}{E_2(n,d_1^*)}\right]G_2(m,n) - \frac{F_2(n,d_1^*)}{E_2(n,d_1^*)} \tag{19}$$

with

$$E_1{'}(m,y^*) = \frac{\partial E_1(m,y^*)}{\partial y^*} \tag{20}$$

$$E_2{'}(n,y^*) = \frac{\partial E_2(n,y^*)}{\partial y^*} \tag{21}$$

10    $$F_1{'}(m,y^*) = \frac{\partial F_1(m,y^*)}{\partial y^*} \tag{22}$$

$$F_2{'}(n,y^*) = \frac{\partial F_2(n,y^*)}{\partial y^*} \tag{23}$$

$$G_1(m,n) = \frac{\int_{l_2^*}^1 sin(\lambda_m x^*)\,cos[\alpha_n(x^*-l_2^*)]dx}{\int_0^1 sin^2(\lambda_m x^*)dx} \tag{24}$$

$$G_2(m,n) = \frac{\int_{l_2^*}^1 sin(\lambda_m x^*)\,cos[\alpha_n(x^*-l_2^*)]dx}{\int_{l_2^*}^1 cos^2[\alpha_n(x^*-l_2^*)]dx} \tag{25}$$

2.4 Transient solution for hydraulic head distribution

15   The semi-analytical solution of the model for transient hydraulic head distribution with the previous steady-state solution as the initial condition is developed via the methods of finite sine transform, finite cosine transform and Laplace transform. The detailed derivation for transient solution is given in Appendix B and the results of the dimensionless hydraulic heads in Laplace domain for regions 1 and 2 are respectively

$$\tilde{\phi}_1^*(x^*,y^*,p) = \delta_1 \sum_{i=1}^{\infty}[w_{1i}^* TE_1(i,y^*,p) + T_1(i,y^*,p) + T_2(i,y^*,p) + SQ_1(i,y^*,p)]\,sin(\lambda_i x^*) \tag{26}$$

20   and

$$\tilde{\phi}_2^*(x^*,y^*,p) = \delta_2 \sum_{j=1}^{\infty}[w_{2j}^* TE_2(j,y^*,p) + T_4(j,y^*,p) + T_5(j,y^*,p) + SQ_2(j,y^*,p)]\,cos[\alpha_j(x^* - l_2^*)] \tag{27}$$

with

$$TE_1(i, y^*, p) = \frac{e^{\mu_i(y^* - d_1^*)} - e^{-\mu_i(y^* + d_1^*)}}{1 - e^{-2\mu_i d_1^*}} \tag{28}$$

$$T_1(i, y^*, p) = \frac{1}{\mu_i p} \left[\theta_1^2 \lambda_i (-1)^i\right] \left[h_{31}^* e^{-\mu_i y^*} + (h_{23}^* y^* - h_{31}^*)\right] - h_{31}^* \frac{(-1)^i}{\lambda_i} e^{-\mu_i y^*} \tag{29}$$

$$T_2(i, y^*, p) = -C_{1m} \left[\frac{1}{2} - \frac{sin(2\lambda_i)}{4\lambda_i}\right] \left[\frac{-e^{-\Omega_{1i}(y^* - d_1^*)} + e^{\Omega_{1i}(y^* - d_1^*)}}{\left(1 - e^{2\Omega_{1i} d_1^*}\right)(\Omega_{1i}^2 - \mu_i^2)} + \frac{\delta_1(-1)^i}{\mu_i^2}(h_{23}^* y^* + h_{31}^* - h_{31}^* e^{-\mu_i y^*})\right] \tag{30}$$

$$SQ_1(i, y^*, p) = \begin{cases} \frac{1}{2\mu_i p} \sum_{k=1}^{M} Q_{1k}^* sin(\lambda_i x_{1k}^*) \frac{1}{1 - e^{-\mu_i d_1^*}} \begin{bmatrix} e^{\mu_i(y_{1k}^* - 2d_1^*)} + e^{\mu_i(y^* - y_{1k}^* - d_1^*)} \\ + e^{\mu_i(y_{1k}^* - y^*)} - e^{\mu_i(y^* - y_{1k}^* - 2d_1^*)} \\ - e^{\mu_i(y_{1k}^* - y^* - d_1^*)} - e^{-\mu_i y_{1k}^*} \end{bmatrix}, y^* > y_{1k}^* \\ \frac{1}{2\mu_i p} \sum_{k=1}^{M} Q_{1k}^* sin(\lambda_i x_{1k}^*) \frac{1}{1 - e^{-\mu_i d_1^*}} \begin{bmatrix} e^{\mu_i(y^* - y_{1k}^*)} + e^{\mu_i(y_{1k}^* - 2d_1^*)} \\ - e^{\mu_i(y^* + y_{1k}^* - 2d_1^*)} - e^{-\mu_i y_{1k}^*} \end{bmatrix}, y^* < y_{1k}^* \end{cases} \tag{31}$$

5    $$TE_2(j, y^*, p) = \frac{e^{-\theta_j y^*} - e^{\theta_j(y^* - 2)}}{e^{-\theta_j d_1^*} - e^{\theta_j(d_1^* - 2)}} \tag{32}$$

$$T_4(j, y^*, p) = \left[\frac{\theta_2^2 \alpha_j(-1)^j}{p} + \frac{S_{s2} K_{y1}(-1)^j}{S_{s1} K_{y2} \alpha_j}\right] \left[\frac{H_{31}^* + H_{23}^* y^* - H_{21}^* e^{\theta_j(y^* - 1)}}{\theta_j^2}\right] + \frac{H_{21}^*}{\alpha_j} \frac{(-1)^j}{p} e^{\theta_j(y^* - 1)} \tag{33}$$

$$T_5(j, y^*, p) = -D_{2n} \frac{S_{s2} K_{y1}(1 - l_2^*)}{2 S_{s1} K_{y2}} \left(\frac{e^{\Omega_{2j}(y^* - 2)} - e^{-\Omega_{2j} y^*}}{\theta_j^2 - \Omega_{2j}}\right) \tag{34}$$

$$SQ_2(j, y^*, p) = \begin{cases} \frac{1}{2\theta_j p} \sum_{l=1}^{N} Q_{2l}^* cos(\alpha_j x_{2l}^*) \left(e^{-\theta_j(y^* - y_{2l}^*)} - e^{-\theta_j(2 - y^* - y_{2l}^*)}\right), y^* > y_{2j}^* \\ \frac{1}{2\theta_j p} \sum_{l=1}^{N} Q_{2l}^* cos(\alpha_j x_{2l}^*) \left(e^{\theta_j(y^* - y_{2l}^*)} - e^{-\theta_j(2 - y^* - y_{2l}^*)}\right), y^* < y_{2j}^* \end{cases} \tag{35}$$

where p is the Laplace variable and the symbols or dimensionless parameters δ_1, δ_2, α_j, λ_i, μ_i, θ_1, θ_2, θ_j, Ω_{1i}, Ω_{2j} and H_{21}^*

10   are introduced in Table 1.

The coefficients in Eqs. (26) and (27) are obtained via continuity requirements for the hydraulic head and flow flux at the interface CF. They can be solved simultaneously based on the following two equations

$$w_{1i}^* = \frac{K_{y2}}{K_{y1}} \frac{h_2}{h_1} G_1(i, j) \sum_{i=1}^{\infty} \frac{w_{2j}^* TE_2'(j, y^*, p) + T_4'(j, y^*, p) + T_5'(j, y^*, p) + SQ_2'(j, y^*, p)}{TE_1'(j, y^*, p)}\bigg|_{y^* = d_1^*} + \sum_{i=1}^{\infty} \frac{-T_1'(j, y^*, p) + T_2'(j, y^*, p) + SQ_1'(j, y^*, p)}{TE_1'(j, y^*, p)}\bigg|_{y^* = d_1^*} \tag{36}$$

and

15   $$w_{2j}^* = \frac{h_1}{h_2} G_2(j, i) \sum_{j=1}^{\infty} \frac{w_{1i}^* TE_1(i, y^*, p) + T_1(i, y^*, p) - T_2(i, y^*, p) + SQ_1(i, y^*, p)}{TE_2(j, y^*, p)}\bigg|_{y^* = d_1^*} - \sum_{j=1}^{\infty} \frac{T_4(j, y^*, p) + T_5(j, y^*, p) + SQ_2(j, y^*, p)}{TE_2(j, y^*, p)}\bigg|_{y^* = d_1^*} \tag{37}$$

with

$$TE_1'(i, y^*, p) = \frac{\partial TE_1(i, y^*, p)}{\partial y^*} \tag{38}$$

$$TE_2'(j, y^*, p) = \frac{\partial TE_2(j, y^*, p)}{\partial y^*} \tag{39}$$

$$T_1'(i, y^*, p) = \frac{\partial T_1(i, y^*, p)}{\partial y^*} \tag{40}$$

$$T_2'(i, y^*, p) = \frac{\partial T_2(i, y^*, p)}{\partial y^*} \tag{41}$$

$$T_4'(j, y^*, p) = \frac{\partial T_4(j, y^*, p)}{\partial y^*} \tag{42}$$

5 $$T_5'(j, y^*, p) = \frac{\partial T_5(j, y^*, p)}{\partial y^*} \tag{43}$$

$$SQ_1'(i, y^*, p) = \frac{\partial SQ_1(i, y^*, p)}{\partial y^*} \tag{44}$$

$$SQ_2'(j, y^*, p) = \frac{\partial SQ_2(j, y^*, p)}{\partial y^*} \tag{45}$$

The coefficient w_{2j}^* can be determined by substituting Eq. (36) into Eq. (37), the w_{1i}^* can then be obtained once w_{2j}^* is known. The hydraulic head distributions in real time domain can be obtained by applying a numerical Laplace inversion scheme, called

10 the Stehfest algorithm (Stehfest, 1970), to Eqs. (26) and (27).

2.5 Stream depletion rate

Pumping in an aquifer near a stream often produces water filtration from the stream toward the well (Yeh et al., 2008). Water extracted by the pumping well comes from the sources such as aquifer storage and nearby streams. The extraction rate from the stream is referred to as stream depletion rate (*SDR*). Since the boundaries AG and ED do not correspond to streams in

15 physical world and are mathematically treated as constant-head because they are far from the pumping well, only the water filtration from streams AB and BD to the nearby pumping well needs to be considered. The dimensionless solutions of *SDR* in Laplace domain from the stream reaches AB and BD, denoted respectively as $\widetilde{SDR}_{AB}$ and $\widetilde{SDR}_{BD}$, can be estimated by taking the derivatives of Eqs. (26) and (27) with respect to *y* and *x*, respectively, then integrating along the reaches as:

$$\widetilde{SDR}_{AB} = \frac{q_A}{Q} = -\frac{1}{Q} \int_0^{l_1} K_{y1} \left. \frac{\partial \tilde{\phi}_1(x, y, p)}{\partial y} \right|_{y=0} dx \tag{46}$$

20 and

$$\widetilde{SDR}_{BD} = \frac{q_B}{Q} = \frac{1}{Q} \left(\int_0^{d_1} K_{x1} \left. \frac{\partial \tilde{\phi}_1(x, y, p)}{\partial x} \right|_{x=l_1} dy + \int_{d_1}^{d_2} K_{x2} \left. \frac{\partial \tilde{\phi}_2(x, y, p)}{\partial x} \right|_{x=l_1} dy \right) \tag{47}$$

Further, the *SDR* solution for streams AB and BD in real time domain are respectively denoted as SDR_{AB} and SDR_{BD} and also obtained by the Stehfest algorithm (Stehfest, 1970). The total dimensionless stream depletion rate (SDR_T) in time domain comes from the streams (AB and BD) is expressed as:

25 $$SDR_T = SDR_{AB} + SDR_{BD} \tag{48}$$

Since the depletion rate from constant-head boundaries AG and DE which are far from the pumping well and can be neglected, the dimensionless storage release rate (SRR) representing the storage release rate due to compression of aquifer matrix and expansion of groundwater in the pore space can be approximated as:

$$SRR = 1 - SDR_T \tag{49}$$

3 Comparisons of present solution, numerical solutions and field observed data

3.1 Comparisons of present solution with MODFLOW solution

The software MODFLOW (USGS, 2005) is used to simulate the groundwater flow due to pumping in the L-shaped aquifer in Yongpoong 2 Agriculture District with different hydraulic conductivities for the two layers. As shown in Figure 1, region 1 has an area of 852 m × 222 m (i.e., $l_1 \times d_1$) while the area of region 2 is 297 m × 183 m (i.e., $(l_1 - l_2) \times (d_2 - d_1)$). Thus, the total area of these two regions is 243495 m^2 which is close to the area of the fluvial aquifer (246500 m^2) reported in Kihm et al. (2007). In the simulation of MODFLOW, the plane of the L-shaped aquifer is discretized with a uniform cell size of 3 m × 3 m. The aquifer thickness is 6 m and divided into two layers. The upper loam layer is 2.5-meter-thick and the lower sand layer is 3.5-meter-thick (Kihm et al. 2007). Within the aquifer domain, there is totally 54110 cells while the numbers of cell are 42032 and 12078 respectively for region 1 and region 2. The boundary conditions specified for the L-shaped aquifer are the same as those defined in the mathematical model. The hydraulic heads along AG and DE are respectively $h_1 = 5.18$ m and $h_2 = 5.29$ m and the head at point B is $h_3 = 4.06$ m. Following Kihm et al. (2007), the fluvial aquifer is considered isotropic and homogeneous in the horizontal direction. In other words, the hydraulic conductivities in x and y directions are identical in both regions 1 and 2 (i.e., $K_{x1} = K_{y1} = K_{x2} = K_{y2} = K$). However, the aquifer is heterogeneous in the vertical direction. It has two layers with hydraulic conductivity $K_U = 3 \times 10^{-6}$ m/s for the upper layer and $K_L = 2 \times 10^{-4}$ m/s for the lower layer. The specific storage of the aquifer in both regions 1 and 2 is 10^{-4} m^{-1} (Kihm et al. 2007). Consider that the pumping well P_w is located at $(609 \text{ m}, 9 \text{ m})$ in region 1 shown in Figure 2 with a rate of 120 m^3/day for one year pumping. Figure 3 shows the hydraulic head distribution obtained from MODFLOW simulations and denoted as the dotted line.

The global behaviour of a multi-layered aquifer may be approximated with that of an equivalent homogeneous medium, whose hydraulic conductivity in the horizontal plane K_h may be evaluated as (Charbeneau, 2000):

$$K_h = \sum_i^m b_i K_i / \sum_i^m b_i \tag{50}$$

where K_i is the hydraulic conductivity in the horizontal direction for layer i, b_i is the thickness of layer i, and m is the number of the layers. Accordingly, the equivalent horizontal hydraulic conductivity K_h for the two layered L-shaped aquifer is estimated as 1.2×10^{-4} m/s. The solid line in Figure 3 represents the hydraulic head distribution predicted by the present solution of Eqs. (26) and (27). The head distribution predicted by the present solution agrees with that of MODFLOW simulations except in the region near the no-flow boundary FG, where has the largest relative deviation 2.1%. The comparison

of the head distributions indicates that the use of equivalent hydraulic conductivity in the present model is appropriate and gives a fairly good predicted results.

3.2 Steady-state head distribution without pumping in Yongpoong 2 Agriculture District and impact of aquifer anisotropy

5   Kihm et al. (2007) reported the steady-state hydraulic head distribution, shown in Figure 4 by the dashed line, for the FEM simulation without groundwater pumping in the two-layered irregular aquifer. Figure 4 also shows the steady-state head distributions predicted by the present solution of Eqs. (11) and (12) denoted as the solid line and by the MODFLOW denoted as dotted line both for the L-shaped aquifer with $K_{x1} = K_{y1} = K_{x2} = K_{y2} = 1.2 \times 10^{-4}$ m/s (i.e., $\kappa_1 = \kappa_2 = 1$) evaluated based on Eq. (50) and other aquifer properties mentioned in Sect. 3.1. Similar to the pumping case, the predicted head

10   distribution of present solution conforms to the results of MODFLOW simulation except in the area near the no-flow boundary FG. The result of present solution shows that the predicted contour lines of the head distribution are nearly parallel to the boundary AG and perpendicular to the boundary FG in the region $x \leq 200$ m. Moreover, the predicted heads within the regions between 500 m $\leq x \leq 852$ m and 0 m $\leq y \leq 200$ m are reasonably close to the FEM results, which range from 4.3 m to 4.7 m as shown in Figure 4. The groundwater flows toward point B since it has the lowest water table within the problem

15   domain.

Figure 5 shows the contour lines of the hydraulic head distribution for isotropic case of $\kappa_1 = \kappa_2 = 1$ by the solid line and for anisotropic cases of $\kappa_1 = \kappa_2 = 4$ represented by the dashed dot line and $\kappa_1 = \kappa_2 = 0.25$ by the dashed line. In these three cases, the head distributions are significantly different in the region where $x \leq 600$ m for the head ranging from 5 m to 4.6 m. The largest head difference occurs near the upper boundary FG, reflecting the effects of no-flow condition and aquifer

20   anisotropy on the flow pattern within this area.

3.3 Spatial head distributions due to pumping simulated by Kihm et al. (2007) and present solution after one year pumping

Figure 3 shows the spatial head distributions in the L-shaped aquifer predicted by the present solution and the MODFLOW for one-year pumping at well P_w located at $(609 \text{ m}, 9 \text{ m})$ with a rate of 120 m^3/day. In fact, Kihm et al. (2007) reported their

25   FEM simulations for head distributions, groundwater flow velocity, and land displacement for one-year pumping at the well P_w with the same pumping rate mentioned above. They referred the simulated head results as initial steady-state distributions for the case of no pumping and final steady-state distributions for the case after one-year pumping. The aquifer configuration in their FEM simulations and the simulated head distributions denoted as dashed line are also demonstrated in Figure 3. The figure indicates that the present solution gives good predicted head contours near the pumping well and reasonably good result

30   for the head distribution in region 1 as compared to those given by Kihm et al. (2007). The head distributions predicted by the FEM solution and present solution have obvious differences in the area far away from the pumping well. Those differences may be mainly caused by the difference in the physical domain considered in FEM solution and the simplified domain used in

the present solution. In addition, the mathematical model in Kihm et al. (2007) considered the unsaturated flow and deformation of the unsaturated soil, which may also affect the head distribution after pumping. Notice that the pumping well is very close to the stream boundary AB, which is the main stream in that area and provides a large amount of filtration water to the well. Hence, both groundwater flows in region 1 for $x \leq 300$ m (near boundary AG) and in region 2 for $y \geq 200$ m (near boundaries DE and EF) are almost not influenced by the pumping because these two regions are far away from the pumping well.

Three piezometers O_1, O_2 and O_3 were respectively installed at $(597\,\text{m}, 25\,\text{m})$, $(594\,\text{m}, 48\,\text{m})$ and $(597\,\text{m}, 204\,\text{m})$ as mentioned in Kihm et al. (2007) and indicated in Figure 2. Note that O_1 was installed near the stream AB while O_3 was far away from the stream but close to the impermeable boundary FG. Figure 6 shows the temporal distributions of hydraulic head measured at these three piezometers (i.e., H_{iO}, $i = 1, 2, 3$) and predicted by the FEM simulations (Kihm et al., 2007) (i.e., H_{iF}), present solution (i.e., H_{iA}) and MODFLOW simulations (i.e., H_{iM}). This figure indicates that the hydraulic heads predicted by the present solution has a good agreement with those simulated by Kihm et al. (2007). The largest relative differences between the temporal hydraulic head predicted by the FEM and present solution are 0.58%, 0.31%, and 0.51% m for O_1, O_2, and O_3, respectively. As shown in Figures 2 and 3, more than half of aquifer boundary is surrounded by perennial streams and constant-head boundaries, and the pumping well is installed close to the main stream AB for stream filtration and screened in the highly permeable sand layer (Kihm, et al. 2007). It is expected that the extracted water from the pumping well mainly comes from the stream AB and the differences of the hydraulic heads from the observations (O_1, O_2, and O_3) between the present solution and FEM simulation are insignificant because the boundary geometry near these observation in both present solution and Kihm et al. (2007) are similar. These difference may be caused by the solid skeleton deformation and unsaturated flow considered in the FEM simulation of Kihm et al. (2007). The Young's modulus (E) of the sand layer is 1.9×10^7 N/m^2 (Kihm et al. 2007), implying that the deformation of sand layer due to pumping may be small. This is also responded in the vertical displacements reported in Kihm et al. (2007). The largest vertical displacement reported in Kihm et al. (2007) is only -0.003 m. Hence, the effect of land displacement during pumping may not significantly influence the hydraulic heads in piezometers. In addition, the unsaturated flow may slightly affect the saturated flow system. This is because the average thickness of unsaturated zone is about 1.26 m, and it consists of a low permeability material (i.e., loam), which is two order less than that of saturated zone (i.e., most of sand). As mentioned earlier, the pumping well is screened in the sand layer and the stream AB is the major source of extracted water. Therefore, the influence of unsaturated zone on the saturated flow may be small. Under such hydrogeological conditions, the present solution yields similar prediction for the temporal hydraulic head distribution as compared with those of FEM. Compared with the field observation, the differences of predicted hydraulic head among FEM, present solution and MODFLOW are all less than 0.08 m at these three piezometers during 0.1 to 10 day. In addition, the largest relative differences between measured heads and predicted heads by the present solution at O_1 to O_3 during 0.1 to 5 day are respectively 1.64%, 1.74% and 0.62%, indicating that the present solution gives good predictions in the early pumping period. Moreover, the effects of unsaturated flow and land deformation on the groundwater flow in Yongpoong aquifer are

small and may be neglected. The hydraulic head at O_1 drops larger than those at O_2 and O_3 whereas the former is located closer to the pumping well P_w. Because P_w is very near the stream, the extracted water will be quickly contributed from the stream and therefore the drawdown at O_1 will be soon stabilized. Figure 6 indicates that the hydraulic heads at O_1 - O_3 predicted by the present solution reach steady state after $t = 100$ days, 220 days and 290 days, respectively.

3.4 Stream filtration in fluvial aquifer systems

Stream filtration can be considered as a problem associated with the interaction between the groundwater and surface water. The pumped water originated from the nearby stream is commonly supplied for irrigation, municipalities, and rural homes. In stream basins with several tributaries, pumping wells are often installed adjacent to the confluence of two tributaries in fluvial aquifers (Lambs, 2004).

It is of practical interest to know the temporal SDR distributions from both streams in the Yongpoong area when subject to pumping at P_w under a rate of 120 m³/day. The distances from P_w to the streams AB and BD are respectively 9 m and 243 m. Figure 7 shows the temporal SDR distribution from each stream, indicating that SDR_{AB} (i.e., SDR from stream AB) is significantly larger than SDR_{BD} (SDR from stream BD) all the time. The steady-state values for SDR_{AB} and SDR_{BD} are respectively 0.81 and 0.19 when $t \geq 220$ day. This is due to the fact that pumping well is closer to stream AB than stream BD and therefore water contributing to the pumping well from stream AB is much more than from stream BD. Figure 7 also shows that the SDR_T is zero and the aquifer storage release rate SRR is unity when $t \leq 0.01$ day, indicating that the well discharges totally from the aquifer storage at early time. Once the drawdown cone reaches the stream, the SDR_T increases quickly with time while the SRR decreases continuously over the entire pumping period. It is interesting to mention that SDR_T starts to contribute more water to the pumping than SRR when $t \geq 5$ day. Finally, the SDR_T reaches unity and the SRR equals zero after $t \geq 220$ days, indicating that the aquifer system approaches steady state and all the extraction water comes from the streams.

4 Conclusions

A new semi-analytical model has been developed to analyze the 2D hydraulic head distributions with/without pumping in a heterogeneous and anisotropic aquifer for an L-shaped domain bounded by two streams with linearly varying hydraulic heads. Method of domain decomposition is used to divide the aquifer into two regions for the development of semi-analytical solution. Steady-state solution is first derived and used as the initial condition for the L-shaped aquifer system before pumping. The Laplace-domain solution of the model for transient head distribution in the aquifer subject to pumping is developed using the Fourier finite sine and cosine transform and the Laplace transform. The solution for SDR describing filtration rate from two streams in an L-shaped aquifer is developed based on the head solution and Darcy's law. The Stehfest algorithm is then adopted to evaluate the time-domain results for both head and SDR solutions in Laplace domain.

The 3D finite difference model MODFLOW is first used to support the evaluation of the hydraulic head predictions by the present solution for the L-shaped two-layered aquifer system. The hydraulic head distributions predicted by present solutions agree fairly well over the entire aquifer except the heads nearing the no-flow boundary. The solution for hydraulic head distribution in the L-shaped aquifer without pumping has been used to investigate the effect of anisotropic ratio (K_x/K_y) on

5   the steady-state flow system. It is interesting to note that the flow pattern in terms of lines of equal hydraulic head is strongly influenced by the value of anisotropic ratio for the region near the turning point of the L-shaped aquifer.

The transient solution for head distribution is employed to simulate the head distribution induced by pumping in the aquifer within the agriculture area of Gyeonggi-Do, Korea. The aquifer is approximated as L-shaped in this study. The present solution delivers fairly good result in predicting the temporal hydraulic head distribution while comparing with those of FEM reported

10   in previous study. Those simulation results seem to indicate that the effects of unsaturated flow and land displacement on the groundwater flow are not significant and may be ignorable. The largest relative differences between the measured heads and the predicted heads by the present solution at three piezometers are less than 1.74%.

The *SDR* solution is first used to evaluate the steady-state *SDR* from each of the nearby streams for Yongpoong aquifer subject to a specific pumping rate. The solution is also employed to determine the temporal contribution rates from the aquifer storage

15   and the streams toward the extraction well.

Acknowledgements

This study was partly supported by the grants from Taiwan Ministry of Science and Technology under the contract numbers MOST 105-2221-E-009-043-MY2 and MOST 106-2221-E-009 -066. The authors would like to thank the editor, two anonymous reviewers, and David Ferris for their valuable and constructive comments that greatly improve the manuscript.

20 **References**

Asadi-Aghbolaghi, M., and Seyyedian, H.: An analytical solution for groundwater flow to a vertical well in a triangle-shaped aquifer, Journal of Hydrology, 393, 341-348, http://dx.doi.org/10.1016/j.jhydrol.2010.08.034, 2010.

Chan, Y. K., Mullineux, N., and Reed, J. R.: Analytic solutions for drawdowns in rectangular artesian aquifers, Journal of Hydrology, 31, 151-160, http://dx.doi.org/10.1016/0022-1694(76)90026-3, 1976.

25   Chan, Y. K., Mullineux, N., and Reed, J. R.: Analytic solution for drawdown in an unconfined-confined rectangular aquifer, Journal of Hydrology, 34, 287-296, http://dx.doi.org/10.1016/0022-1694(77)90136-6, 1977.

Chan, Y. K., Mullineux, N., Reed, J. R., and Wells, G. G.: Analytic solutions for drawdowns in wedge-shaped artesian aquifers, Journal of Hydrology, 36, 233-246, http://dx.doi.org/10.1016/0022-1694(78)90146-4, 1978.

Charbeneau, R. J.: Groundwater Hydraulics and Pollutant Transport, Prentice Hall, Upper Saddle River, N.J, 2000.

Chen, Y.J., Yeh, H. D., and Yang, S. Y.: Analytical Solutions for Constant-Flux and Constant-Head Tests at a Finite-Diameter Well in a Wedge-Shaped Aquifer, Journal of Hydraulic Engineering, 135, 333-337, 10.1061/(ASCE)0733-9429(2009)135:4(333), 2009.

Chu, Y. J., Lin, C. C., and Yeh, H. D.: Steady-state groundwater flow in an anisotropic aquifer with irregular boundaries. International Conference on Sustainable Environmental Technologies, Bangkok, Thailand. 2012

Corapcioglu, M. Y., Borekci, O., and Haridas, A.: Analytical solutions for rectangular aquifers with third-kind (Cauchy) boundary conditions, Water Resources Research, 19, 523-528, 10.1029/WR019i002p00523, 1983.

Daly, C. J., and Morel-Seytoux, H. J.: An integral transform method for the linearized Boussinesq Groundwater Flow Equation, Water Resources Research, 17, 875-884, 10.1029/WR017i004p00875, 1981.

Falade, G. K.: On the flow of fluid in the wedged anisotropic porous domain, Journal of Hydrology, 58, 111-121, http://dx.doi.org/10.1016/0022-1694(82)90072-5, 1982.

Holzbecher, E.: Analytical solution for two-dimensional groundwater flow in presence of two isopotential lines, Water Resources Research, 41, n/a-n/a, 10.1029/2005WR004583, 2005.

Huang, C. S., Chen, J. J., and Yeh, H. D.: Approximate analysis of three-dimensional groundwater flow toward a radial collector well in a finite-extent unconfined aquifer, Hydrol. Earth Syst. Sci., 20, 55-71, 10.5194/hess-20-55-2016, 2016.

Jafari, F., Javadi, S., Golmohammadi, G., Karimi, N., and Mohammadi, K.: Numerical simulation of groundwater flow and aquifer-system compaction using simulation and InSAR technique: Saveh basin, Iran, Environmental Earth Sciences, 75, 833, 10.1007/s12665-016-5654-x, 2016.

Kantorovich, L.V., Krylov, V. I.: Approximate Methods of Higher Analysis. Interscience, New York, 1958.

Kacimov, A. R., Kayumov, I. R., Al-Maktoumi, A.: Rainfall induced groundwater mound in wedge-shaped promontories: The Strack–Chernyshov model revisited. Advances in Water Resources, 97, 110–119, http://dx.doi.org/10.1016/j.advwatres.2016.08.011, 2016.

Kacimov, A. R., Maklakov, D. V., Kayumov, I. R., Al-Futaisi, A.: Free Surface flow in a microfluidic corner and in an unconfined aquifer with accretion: The Signorini and Saint-Venant analytical techniques revisited. Transport in Porous Media, 116(1), DOI 10.1007/s11242-016-0767-y, 115–142, 2017.

Kihm, J.-H., Kim, J.-M., Song, S.-H., and Lee, G.-S.: Three-dimensional numerical simulation of fully coupled groundwater flow and land deformation due to groundwater pumping in an unsaturated fluvial aquifer system, Journal of Hydrology, 335, 1-14, http://dx.doi.org/10.1016/j.jhydrol.2006.09.031, 2007.

Kuo, M. C. T., Wang, W. L., Lin, D. S., Lin, C. C., and Chiang, C. J.: An Image-Well Method for Predicting Drawdown Distribution in Aquifers with Irregularly Shaped Boundaries, Ground Water, 32, 794-804, 10.1111/j.1745-6584.1994.tb00921.x, 1994.

Lambs, L.: Interactions between groundwater and surface water at river banks and the confluence of rivers, Journal of Hydrology, 288, 312-326, http://dx.doi.org/10.1016/j.jhydrol.2003.10.013, 2004.

Latinopoulos, P.: Well recharge in idealized rectangular aquifers, Advances in Water Resources, 5, 233-235, http://dx.doi.org/10.1016/0309-1708(82)90006-9, 1982.

Latinopoulos, P.: Periodic recharge to finite aquifers from rectangular areas, Advances in Water Resources, 7, 137-140, http://dx.doi.org/10.1016/0309-1708(84)90043-5, 1984.

5 Latinopoulos, P.: Analytical solutions for periodic well recharge in rectangular aquifers with third-kind boundary conditions, Journal of Hydrology, 77, 293-306, http://dx.doi.org/10.1016/0022-1694(85)90213-6, 1985.

Li, P., Stagnitti, F., and Das, U.: A new analytical solution for Laplacian porous-media flow with arbitrary boundary shapes and conditions, Mathematical and Computer Modelling, 24, 3-19, http://dx.doi.org/10.1016/S0895-7177(96)00160-4, 1996.

Li, H., and Jiao, J. J.: Tidal groundwater level fluctuations in L-shaped leaky coastal aquifer system, Journal of Hydrology,
10 268, 234-243, http://dx.doi.org/10.1016/S0022-1694(02)00177-4, 2002.

Loudyi, D., Falconer, R. A., and Lin, B.: Mathematical development and verification of a non-orthogonal finite volume model for groundwater flow applications, Advances in Water Resources, 30, 29-42, 10.1016/j.advwatres.2006.02.010, 2007.

Lu, C., Xin, P., Li, L., and Luo, J.: Steady state analytical solutions for pumping in a fully bounded rectangular aquifer, Water Resources Research, 51, 8294-8302, 10.1002/2015WR017019, 2015.

15 Matthews, C. S., Brons, F., and Hazebroek, P.: A method for determination of average pressure in bounded reservoir, Trans. AIME, 201, 182-191, 1954.

Mackowski, D. W.: Conduction Heat Transfer: Notes for MECH 7210. Mechanical Engineering Department, Auburn University, 2011.

Mahdavi, A., Seyyedian, H.: Steady-state groundwater recharge in trapezoidal-shaped aquifers: A semi-analytical approach
20 based on variational calculus. Journal of Hydrology, 512, 457–462, https://doi.org/10.1016/j.jhydrol.2014.03.014, 2014.

Mohanty, S., Jha, M. K., Kumar, A., and Panda, D. K.: Comparative evaluation of numerical model and artificial neural network for simulating groundwater flow in Kathajodi–Surua Inter-basin of Odisha, India, Journal of Hydrology, 495, 38-51, http://dx.doi.org/10.1016/j.jhydrol.2013.04.041, 2013.

Patel, A., and Serrano, S. E.: Decomposition solution of multidimensional groundwater equations, Journal of Hydrology, 397,
25 202-209, http://dx.doi.org/10.1016/j.jhydrol.2010.11.032, 2011.

Read, W. W., and Volker, R. E.: Series solutions for steady seepage through hillsides with arbitrary flow boundaries, Water Resources Research, 29, 2871-2880, 10.1029/93WR00905, 1993.

Rhms 2013, available at: http://mobile.river.go.kr/Mobiles/sub_03/Books/%ED%95%9C%EA%B5%AD%ED%95%98%EC%B2%9C%EC%9D%B
30 C%EB%9E%8C(2012.12.31%EA%B8%B0%EC%A4%80).pdf, last accessed on 04 September 2017. (in Korean)

Samani, N., and Zarei-Doudeji, S.: Capture zone of a multi-well system in confined and unconfined wedge-shaped aquifers, Advances in Water Resources, 39, 71-84, http://dx.doi.org/10.1016/j.advwatres.2012.01.004, 2012.

Samani, N., and Sedghi, M. M.: Semi-analytical solutions of groundwater flow in multi-zone (patchy) wedge-shaped aquifers, Advances in Water Resources, 77, 1-16, http://dx.doi.org/10.1016/j.advwatres.2015.01.003, 2015.

Serrano, S. E.: A simple approach to groundwater modelling with decomposition, Hydrological Sciences Journal, 58, 177-185, 10.1080/02626667.2012.745938, 2013.

Stehfest, H.: Algorithm 368: Numerical inversion of Laplace transforms, Commun. ACM, 13, 47-49, 10.1145/361953.361969, 1970.

5 Sun, H.: A two-dimensional analytical solution of groundwater response to tidal loading in an estuary, Water Resources Research, 33, 1429-1435, 10.1029/97WR00482, 1997.

Taigbenu, A. E.: Green element simulations of multiaquifer flows with a time-dependent Green's function, Journal of Hydrology, 284, 131-150, http://dx.doi.org/10.1016/j.jhydrol.2003.07.002, 2003.

Todd, D. K., and Mays, L. W.: Groundwater Hydrology, 3rd ed, Wiley, 2005.

10 U.S. Geological Survey: MODFLOW-2005: The U.S. geological survey modular groundwater model- the groundwater flow process. U.S. Geological Survey Techniques and Methods 6-A16, 2005

Younger, P. L.: Groundwater in the Environment: An Introduction, 1st ed, Wiley, 2007.

Yeh, H.-D., Chang, Y.-C., and Zlotnik, V. A.: Stream depletion rate and volume from groundwater pumping in wedge-shape aquifers, Journal of Hydrology, 349, 501-511, http://dx.doi.org/10.1016/j.jhydrol.2007.11.025, 2008.

15   Appendix A. Steady-state solution for flow in an L-shaped aquifer without pumping

On the basis of dimensionless variables and parameters defined in Sect. 2.2, Eqs. (1) and (2) can be written respectively as

$$\kappa_1 \frac{b_2^2}{l_1^2}\frac{\partial^2 \phi_1^*}{\partial x^{*2}} + \frac{\partial^2 \phi_1^*}{\partial y^{*2}} = \frac{\partial \phi_1^*}{\partial t^*} - \sum_{k=1}^{M} Q_{1k}^* \delta(x^* - x_{1k}^*)\delta(y^* - y_{1k}^*)$$

$$0 \leq x^* \leq l_1^*, 0 \leq y^* \leq d_1^* \tag{A1}$$

and

$$20 \quad \kappa_2 \frac{d_2^2}{l_1^2}\frac{\partial^2 \phi_2^*}{\partial x^{*2}} + \frac{\partial^2 \phi_2^*}{\partial y^{*2}} = \frac{S_{s2}}{S_{s1}}\frac{K_{y1}}{K_{y2}}\frac{\partial \phi_2^*}{\partial t^*} - \sum_{l=1}^{N} Q_{2l}^* \delta(x^* - x_{2l}^*)\delta(y^* - y_{2l}^*)$$

$$0 \leq x^* \leq l_2^*, d_1^* \leq y^* \leq 1 \tag{A2}$$

The dimensionless boundary conditions for region 1 can be expressed as:

$$\phi_1^*(0, y^*) = 0 \text{ for boundary AG} \tag{A3}$$

$$\phi_1^*(1, y^*) = h_{31}^* + h_{23}^* y^* \text{ for boundary BC} \tag{A4}$$

$$25 \quad \phi_1^*(x^*, 0) = h_{31}^* x^* \text{ for boundary AB} \tag{A5}$$

$$\frac{\partial \phi_1^*}{\partial y^*}(x^*, d_1^*) = 0 \text{ for FG} \tag{A6}$$

and for region 2 are

$$\frac{\partial \phi_2^*}{\partial x^*}(l_2^*, y^*) = 0 \text{ for boundary EF} \tag{A7}$$

$$\phi_2^*(1, y^*) = h_{31}^* + h_{23}^* y^* \text{ for boundary CD} \tag{A8}$$

$$\phi_2^*(x^*, 1) = h_{21}^* \text{ for boundary DE} \tag{A9}$$

5 The continuity requirements of hydraulic head and flux at the region interface in dimensionless form are respectively expressed as

$$h_1 \phi_1^*(x^*, d_1^*) = h_2 \phi_2^*(x^*, d_1^*) \text{ for segment CF} \tag{A10}$$

and

$$K_{y1} h_1 \left.\frac{\partial \phi_1^*}{\partial y^*}\right|_{y^*=d_1^*} = K_{y2} h_2 \left.\frac{\partial \phi_2^*}{\partial y^*}\right|_{y^*=d_1^*} \text{ for segment CF} \tag{A11}$$

10 The steady-state solution for groundwater flow in an L-shaped aquifer without pumping can be solved after removing the source/sink term in Eqs. (A1) and (A2). Multiplying Eq. (A1) by $sin(\lambda_m x^*)$ and integrating it for x^* from 0 to 1 in region 1 with boundary conditions Eqs. (A3) and (A4), Eq. (A1) is then transformed to

$$\Omega_{1m}^2 \bar{\phi}_1^* - \frac{\partial^2 \bar{\phi}_1^*}{\partial y^{*2}} = -\kappa_1 \frac{d_2^2}{l_1^2} \lambda_m (-1)^m (h_{31}^* + h_{23}^* y^*) \tag{A12}$$

with

15 $$\bar{\phi}_1^* = \int_0^1 \phi_1^* sin(\lambda_m x^*) dx^* \tag{A13}$$

where $\Omega_{1m} = \lambda_m \sqrt{\kappa_1} \, d_2 / l_1$, $\lambda_m = m\pi$ and $m = 1, 2, 3, ...$

Similarly, Eq. (A2) can be transformed via multiplying Eq. (A2) by $cos[\alpha_n(x^* - l_2^*)]$ and integrating it for x^* from l_2^* to 1 in region 2 with boundary conditions Eqs. (A7) and (A8). The result is

$$\Omega_{2n}^2 \bar{\phi}_2^* - \frac{\partial^2 \bar{\phi}_2^*}{\partial y^{*2}} = \kappa_2 \frac{d_2^2}{l_1^2} \alpha_n (-1)^{n-1} (H_{31}^* + H_{23}^* y^*) \tag{A14}$$

20 with

$$\bar{\phi}_2^* = \int_{l_2^*}^1 \phi_2^* cos[\alpha_n(x^* - l_2^*)] dx^* \tag{A15}$$

where $\Omega_{2n} = \alpha_n \sqrt{\kappa_2} \, d_2 / l_1$, $\alpha_n = (n - 1/2)\pi/(1 - l_2^*)$ and $n = 1,2,3, ...$

The general solutions of Eqs. (A12) and (A14) can be written respectively as

$$\bar{\phi}_1^*(m, y^*) = C_{1m} e^{\Omega_{1m} y^*} + C_{2m} e^{-\Omega_{1m} y^*} - \frac{(-1)^m}{\lambda_m}(h_{31}^* + h_{23}^* y^*) \tag{A16}$$

and

$$\bar{\phi}_2^*(n, y^*) = D_{1n}e^{\Omega_{2n}y^*} + D_{2n}e^{-\Omega_{2n}y^*} - \frac{(-1)^{n-1}}{\alpha_n}(H_{31}^* + H_{23}^*y^*) \tag{A17}$$

The coefficients C_{1m} and C_{2m} in Eq. (A16) are determined by Eq. (A5) and the result is

$$C_{2m} = -C_{1m} \tag{A18}$$

5   Similarly, the coefficients D_{1n} and D_{2n} in Eq. (A17) are determined based on Eq. (A10) as

$$D_{1n} = -D_{2n}e^{-2\Omega_{2n}} \tag{A19}$$

Substituting Eq. (A18) into Eq. (A16), the inversion of $\bar{\phi}_1^*$ leads to Eq. (12) for dimensionless hydraulic head distribution in region 1. Similarly, the inversion of $\bar{\phi}_2^*$ for region 2 after substituting Eq. (A19) into Eq. (A17) results in Eq. (13). Based on Eqs. (A10) and (A11), the coefficients of C_{1m} and D_{2n} can be simultaneously determined and the results are respectively

10   given in Eqs. (18) and (19).

Appendix B. Transient solutions for an L-shaped aquifer

Multiplying Eq. (A1) by $sin(\lambda_i x^*)$ and integrating it for x^* from 0 to 1 in region 1 with Eqs. (A3) and (A4), Eq. (A1) can be transformed as

$$-\Omega_{1i}^2\bar{\phi}_1^* - \theta_1^2\lambda_i(-1)^i(h_{31}^* + h_{23}^*y^*) + \frac{\partial^2\bar{\phi}_1^*}{\partial y^{*2}} = \frac{\partial\bar{\phi}_1^*}{\partial t^*} - \sum_{k=1}^{M}Q_{1k}^* sin(\lambda_i x_{1k}^*)\,\delta(y^* - y_{1k}^*) \tag{B1}$$

15   with

$$\bar{\phi}_1^* = \int_0^1 \phi_1^* sin(\lambda_i x_{1k}^*)\,dx^* \tag{B2}$$

where $\Omega_{1i} = \lambda_i\sqrt{\kappa_1}\,d_2/l_1$, $\theta_1 = \sqrt{\kappa_1}d_2/l_1$, and $\lambda_i = i\pi$, $i = 1,2,3, \dots$.

Similarly, Eq. (A2) can be transformed via multiplying Eq. (A2) by $cos(\alpha_j x^*)$ and integrating it for x^* from l_2^* to 1 in region 2 with Eqs. (A7) and (A8). The result is

20   $$-\Omega_{2j}^2\bar{\phi}_2^* + \theta_2^2\alpha_j(-1)^j(H_{31}^* + H_{23}^*y^*) + \frac{\partial^2\bar{\phi}_2^*}{\partial y^{*2}} = \frac{K_{y1}S_{s2}}{K_{y2}S_{s1}}\frac{\partial\bar{\phi}_2^*}{\partial t^*} - \sum_{l=1}^{N}Q_{2l}^* cos(\alpha_j x_{2l}^*)\,\delta(y^* - y_{2l}^*) \tag{B3}$$

with

$$\bar{\phi}_2^* = \int_{l_2^*}^1 \phi_2^* cos(\alpha_j x_{2l}^*)\,dx^* \tag{B4}$$

where $\Omega_{2j} = \alpha_j\sqrt{\kappa_2}d_2/l_1$, $\theta_2 = \sqrt{\kappa_2}d_2/l_1$, and $\alpha_j = (1 - 1/2)\pi/(1 - l_2^*)$ for $j = 1,2,3, \dots$.

Then, taking Laplace transforms to Eq. (B1) results in

$$-\Omega_{1i}^2 \bar{\bar{\phi}}_1^* - \frac{1}{p}\theta_1^2\lambda_i(-1)^i(h_{31}^* + h_{23}^*y^*) + \frac{\partial^2\bar{\bar{\phi}}_1^*}{\partial y^{*2}} = p\bar{\bar{\phi}}_1^* - \bar{\phi}_{1s}^* - \frac{1}{p}\sum_{k=1}^{M}Q_{1k}^* \sin(\lambda_i x_{1k}^*)\,\delta(y^* - y_{1k}^*) \tag{B5}$$

where $\bar{\phi}_{1s}^*$ is the steady state solution of region 1. Hence, Eq. (B5) can be organized as:

$$-\mu_i^2 + \bar{\bar{\phi}}_1^* + \frac{\partial^2\bar{\bar{\phi}}_1^*}{\partial y^{*2}} = \frac{1}{p}\theta_1^2\lambda_i(-1)^i(h_{31}^* + h_{23}^*y^*) - \sum_{m=1}^{\infty}\Delta_1[C_{1m}E_1(m, y^*) + F_1(m, y^*)]\left(\frac{1}{2} - \frac{sin2\lambda_i}{4\lambda_i}\right) -$$

$$\frac{1}{p}\sum_{k=1}^{M}Q_{1k}^*\sin(\lambda_i x_{1k}^*)\,\delta(y^* - y_{1k}^*) \tag{B6}$$

5   where $\mu_i = \sqrt{\theta_1^2\lambda_i^2 + p}$ with the Laplace transform of $\bar{\phi}_1^*$ defined as:

$$\bar{\bar{\phi}}_1^*(i, y^*, p) = \int_0^{\infty}\bar{\phi}_1^*(i, y^*, t)e^{-pt^*}dt^* \tag{B7}$$

Similarly, the Laplace transform of Eq. (B3) is obtained as:

$$-\Omega_{2j}^2\bar{\phi}_2^* + \frac{1}{p}\theta_2^2\alpha_j(-1)^j(H_{31}^* + H_{23}^*y^*) + \frac{\partial^2\bar{\phi}_2^*}{\partial y^{*2}} = \frac{K_{y1}S_{s2}}{K_{y2}S_{s1}}(p\bar{\bar{\phi}}_2^* - \bar{\phi}_{2s}^*) - \frac{1}{p}\sum_{l=1}^{N}Q_{2l}^*\cos(\alpha_j x_{2l}^*)\,\delta(y^* - y_{2l}^*) \tag{B8}$$

where $\bar{\phi}_{2s}^*$ is the steady state solution of region 2. Thus, Eq. (B8) can be written as:

10   $$-\theta_j^2\bar{\bar{\phi}}_2^* + \frac{\partial^2\bar{\bar{\phi}}_2^*}{\partial y^{*2}} = -\frac{1}{p}\theta_2^2\alpha_j(-1)^j(H_{31}^* + H_{23}^*y^*) - \frac{K_{y1}S_{s2}}{K_{y2}S_{s1}}\sum_{n=1}^{\infty}\Delta_2[D_{2n}E_2(m, y^*) + F_2(m, y^*)]\cos[\alpha_j(x^* - l_2^*)] -$$

$$\frac{1}{p}\sum_{l=1}^{N}Q_{2l}^*\cos(\alpha_j x_{2l}^*)\,\delta(y^* - y_{2l}^*) \tag{B9}$$

where $\theta_j = \sqrt{\theta_2^2\alpha_j^2 + ps_{s2}k_{y1}/s_{s1}k_{y2}}$ with the Laplace transform of $\bar{\phi}_2^*$ defined as:

$$\bar{\bar{\phi}}_2^*(j, y^*, p) = \int_0^{\infty}\bar{\phi}_2^*(j, y^*, t)e^{-pt^*}dt^* \tag{B10}$$

The general solution of Eq. (B6) can be expressed as:

15   $$\bar{\bar{\phi}}_1^*(i, y^*, p) = T_{1i}e^{\mu_i y^*} + T_{2i}e^{-\mu_i y^*} + \bar{\bar{\phi}}_{1p}^*(i, y^*, p) \tag{B11}$$

where the particular solution $\bar{\bar{\phi}}_{1p}^*(i, y^*, p)$ is

$$\bar{\bar{\phi}}_{1p}^*(i, y^*, p) = \frac{e^{\mu_i y^*}}{2\mu_i}\int e^{-\mu_i y^*}\Delta_{1y}(i, y^*, p)dy^* - \frac{e^{-\mu_i y^*}}{2\mu_i}\int e^{\mu_i y^*}\Delta_{1y}(i, y^*, p)dy^* \tag{B12}$$

with

$$\Delta_{1y}(i, y^*, p) = \frac{1}{p}\theta_1^2\lambda_i(-1)^i(h_{31}^* + h_{23}^*y^*) - \sum_{m=1}^{\infty}\Delta_1[C_{1m}E_1(m, y^*) + F_1(m, y^*)]\left(\frac{1}{2} - \frac{sin2\lambda_i}{4\lambda_i}\right) -$$

20   $$\frac{1}{p}\sum_{k=1}^{M}Q_{1k}^*\sin(\lambda_i x_{1k}^*)\,\delta(y^* - y_{1k}^*) \tag{B13}$$

Moreover, Eq. (B9) can also be expressed as:

$$\bar{\bar{\phi}}_2^*(j, y^*, p) = T_{1j}e^{\theta_j y^*} + T_{2j}e^{-\theta_j y^*} + \bar{\bar{\phi}}_{2p}^*(j, y^*, p) \tag{B14}$$

in which $\bar{\bar{\phi}}_{2p}^*(j, y^*, p)$ is

$$\bar{\bar{\phi}}_{2p}^*(j, y^*, p) = \frac{e^{\theta_j y^*}}{2\theta_j}\int e^{-\theta_j y^*}\Delta_{2y}(j, y^*, p)dy^* - \frac{e^{-\theta_j y^*}}{2\theta_j}\int e^{\theta_j y^*}\Delta_{2y}(i, y^*, p)dy^* \tag{B15}$$

with

$$\Delta_{2y}(j, y^*, p) = -\frac{1}{p}\theta_2^2\alpha_j(-1)^j(H_{31}^* + H_{23}^* y^*) - \frac{K_{y1}S_{s2}}{K_{y2}S_{s1}}\sum_{n=1}^{\infty}\Delta_2[D_{2n}E_2(m, y^*) + F_2(m, y^*)]\cos[\alpha_j(x^* - l_2^*)] -$$

$$\frac{1}{p}\sum_{l=1}^{N}Q_{2l}^*\cos(\alpha_j x_{2l}^*)\delta(y^* - y_{2l}^*) \tag{B16}$$

On the basis of Eq. (A5), the coefficient T_{2i} in Eq. (B11) can be determined in terms of T_{1i} as:

$$T_{2i} = -h_{31}^*\frac{(-1)^i}{\lambda_i} + \frac{h_{31}^*}{p\mu_i^2}[\theta_1^2\lambda_i(-1)^i] + \Delta_1(-1)^i C_{1m}\left(\frac{1}{2} - \frac{\sin 2\lambda_i}{4\lambda_i}\right) - T_{1i} \tag{B17}$$

The solution for hydraulic head distribution in region 1 is given as Eq. (26) which is obtained by substituting Eq. (B17) into Eq. (B11) and then taking the following inverse Fourier transform to Eq. (B11) denoted as:

$$\tilde{\phi}_1^*(x^*, y^*, p) = \sum_{i=0}^{\infty}\bar{\bar{\phi}}_1^*(i, y^*, p)\sin(\lambda_i x^*) \tag{B18}$$

with

$$w_{1i}^* = T_{1i}(e^{\mu_i y^*} - 1)\big|_{y^* = d_1^*} - \frac{1}{2\mu_i p}\sum_{k=1}^{M}Q_{1k}^*\sin(\lambda_i x_{1k}^*)[e^{\mu_i(y^* - y_{1k}^*)} - e^{\mu_i(y_{1k}^* - y^*)}]\big|_{y^* = d_1^*} \tag{B19}$$

Similarly, T_{1j} in Eq. (B14) can be obtained based on Eq. (A9) as:

$$T_{1j} = T_{2j}e^{-2\theta_j} - \left[\frac{\theta_2^2\alpha_j(-1)^j}{p} + \frac{K_{y1}S_{s2}(-1)^j}{K_{y2}S_{s1}\alpha_j}\right]\frac{H_{21}^*e^{-\theta_j}}{\theta_j^2} + \frac{H_{21}^*e^{-\theta_j}(-1)^j}{\alpha_j p} + \frac{1}{p}\sum_{l=1}^{N}Q_{2l}^*\cos(\alpha_j x_{2l}^*)\frac{e^{-\theta_j y_{2l}^*} - e^{\theta_j(y_{2l}^* - 2)}}{2\theta_j} \tag{B20}$$

The solution for region 2 is Eq. (27) which is acquired by substituting Eq. (B20) into Eq. (B14) then taking the following inverse Fourier transform to Eq. (B14) expressed as:

$$\tilde{\phi}_2^*(x^*, y^*, p) = \sum_{j=0}^{\infty}\bar{\bar{\phi}}_2^*(j, y^*, p)\cos(\alpha_j x^*) \tag{B21}$$

with

$$w_{2j}^* = T_{2j} \tag{B22}$$

Furthermore, the coefficients of w_{1i}^* and w_{2j}^* can be simultaneously determined by Eqs. (A10) and (A11). The results are respectively given in Eqs. (36) and (37).

Table 1 Notations used in the text.

Notation	Definition
$\phi_1,\ \phi_2$	Hydraulic head for region 1 and 2. [L]
$Q_{1k},\ Q_{2k}$	Unit thickness pumping rate for region 1 and 2. [L^2/T]
$S_{s1},\ S_{s2}$	Specific storage for region 1 and 2. [L^{-1}]
$K_x,\ K_y$	Hydraulic conductivities in x- and y-direction. [L/T]
t	Time. [T]
p	Laplace variable.
$h_1,\ h_2,\ h_3$	Hydraulic heads at boundaries AG, DE and point B, respectively. [L]
$l_1,\ l_2$	Length of boundary FG and AB. [L]
$d_1,\ d_2$	Length of boundary BC and CD. [L]
$\kappa_1,\ \kappa_2$	Anisotropic ratio of hydraulic conductivity in region 1 and 2.
Δ_1	$\begin{cases}1, & m=0 \\ 2, & m\neq 0\end{cases}, m=1,2,3,\ldots.$
Δ_2	$\frac{2}{1-l_2^*}.$
λ_v	$\frac{v\pi}{l_1^*}, v=m, i=1,2,3,\ldots.$
α_w	$\frac{(w-1/2)\pi}{1-l_2^*}, w=n, j=1,2,3,\ldots.$
Ω_{1v}	$\lambda_v\sqrt{\kappa_1}\,d_2/l_1\,, v=m, i=1,2,3,\ldots.$
Ω_{2w}	$\alpha_w\sqrt{\kappa_2}\,d_2/l_1\,, w=n, j=1,2,3,\ldots.$
$h_{21}{}^*$	$(h_2-h_1)/h_1$
$h_{23}{}^*$	$(h_2-h_3)/h_1$
$h_{31}{}^*$	$(h_3-h_1)/h_1$
$H_{21}{}^*$	$(h_2-h_1)/h_2$
$H_{23}{}^*$	$(h_2-h_3)/h_2$
$H_{31}{}^*$	$(h_3-h_1)/h_2$

δ_1	2
δ_2	$\dfrac{2}{1 - l_2^*}$
θ_1	$\sqrt{\kappa_1(d_2^2/l_1^2)}$
θ_2	$\sqrt{\kappa_2(d_2^2/l_1^2)}$
μ_i	$\sqrt{\theta_1^2 \lambda_i^2 + p}, i = 1,2,3,\dots$
θ_j	$\sqrt{\theta_2^2 \alpha_j^2 + p s_{s2} k_{y1}/s_{s1} k_{y2}}, j = 1,2,3,\dots$

Figures

Figure 1: Location of the fluvial aquifer. Note that this figure is modified from Google Earth.
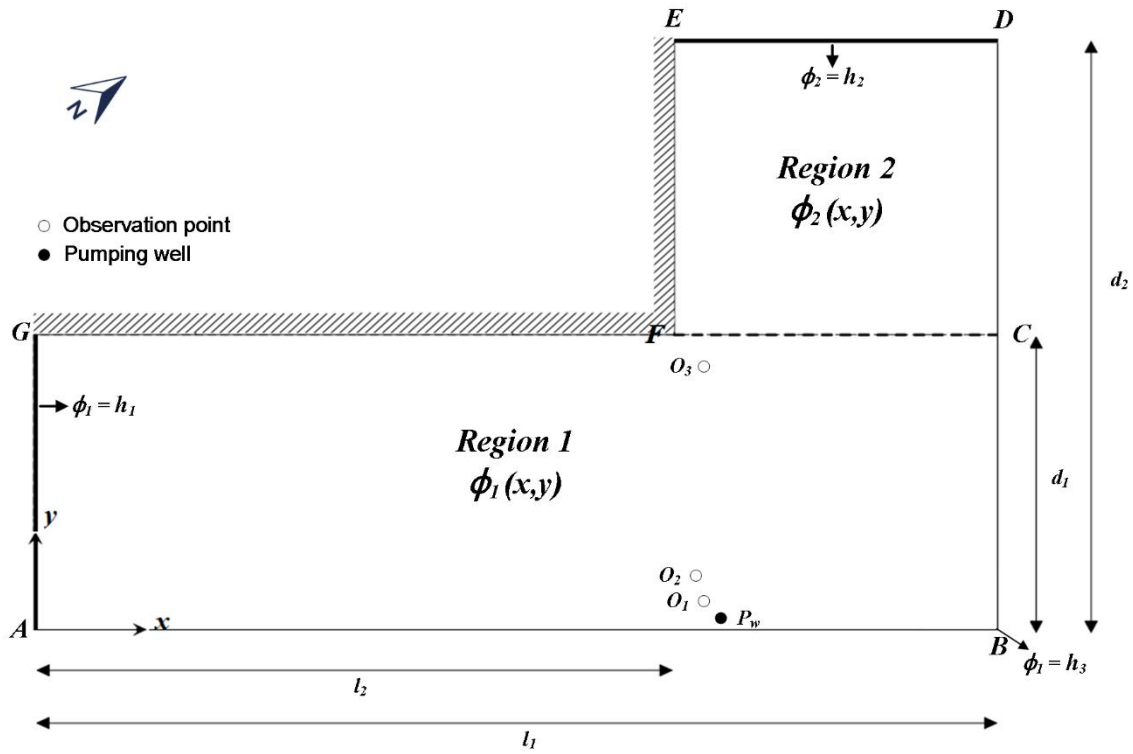
Figure 2: The L-Shaped fluvial aquifer with two sub-regions.
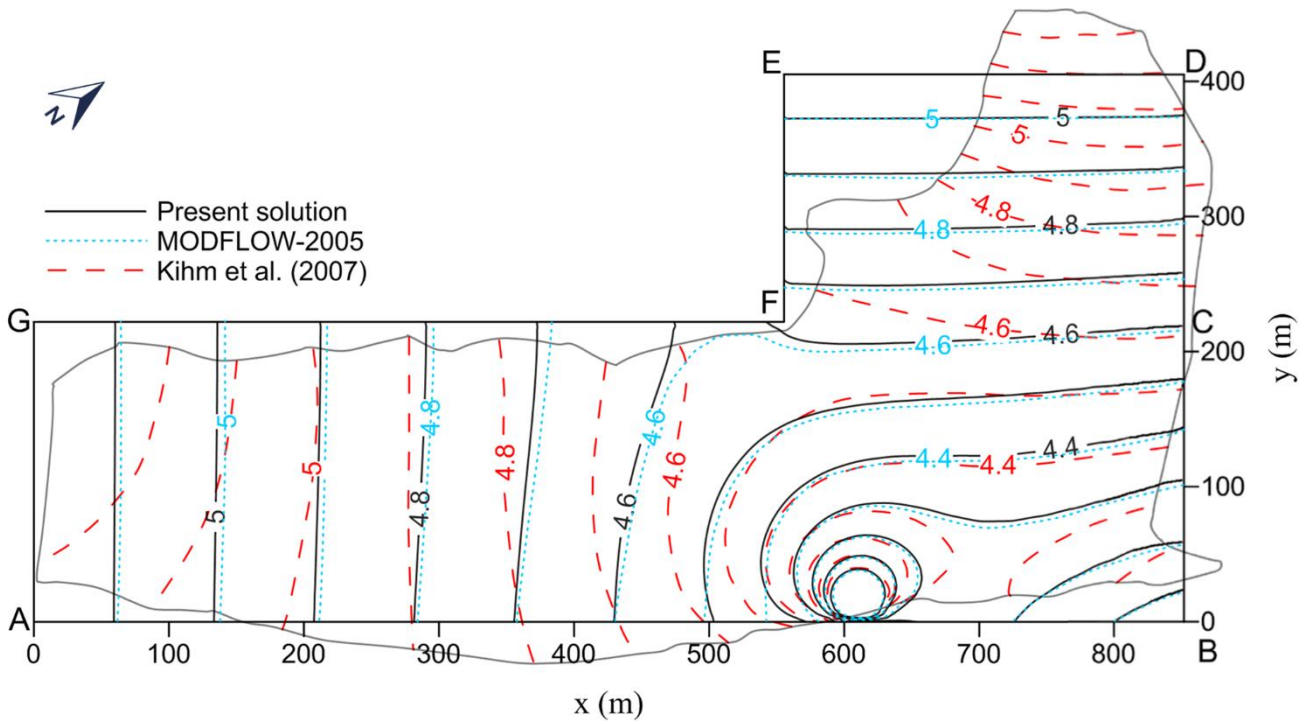
Figure 3: Contours of hydraulic head in L-shaped aquifer predicted by the present solution, MODFLOW, and FEM simulations with irregular outer boundary reported in Kihm et al. (2007).
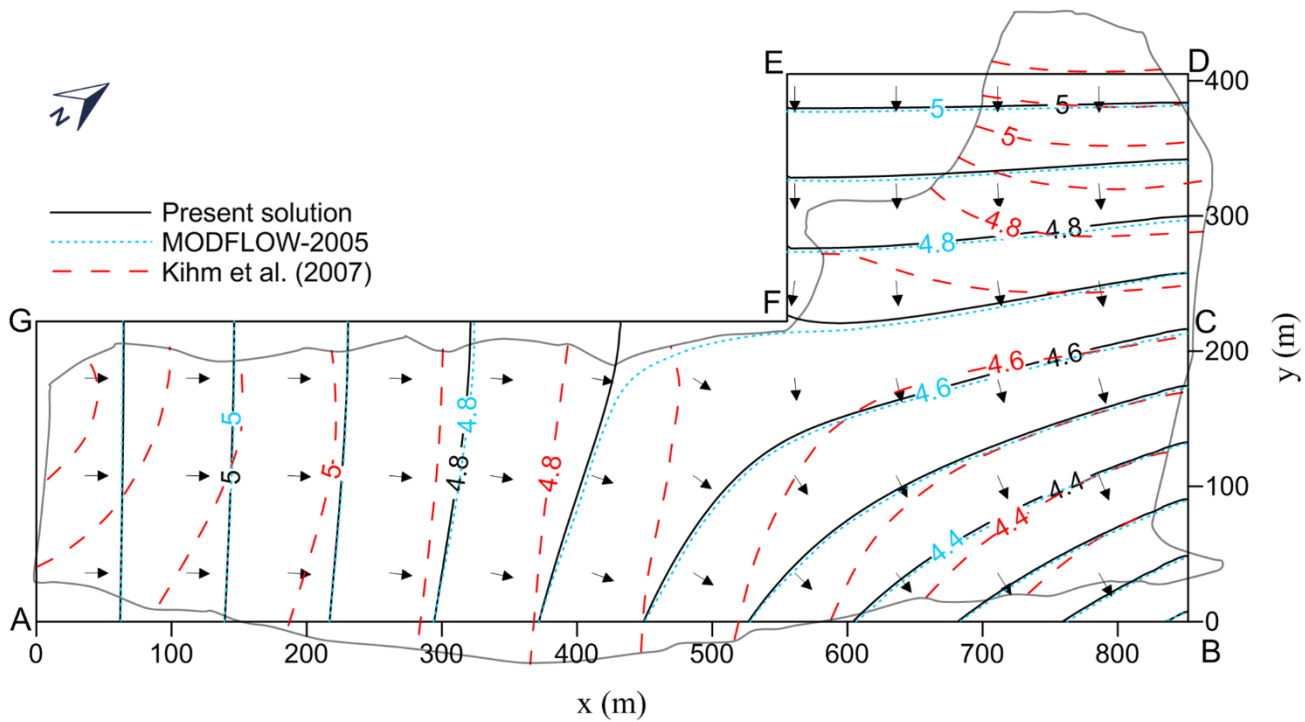
Figure 4: Steady-state hydraulic head contours without pumping in Yongpoong 2 Agriculture District.
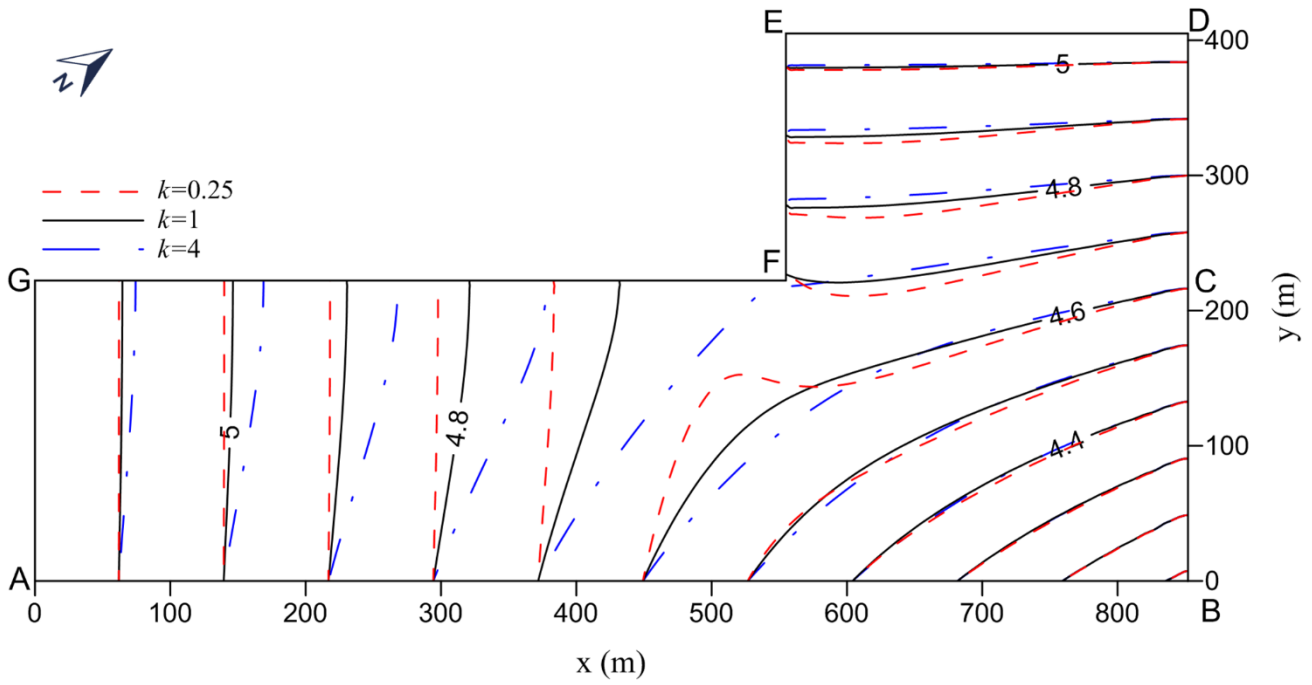
Figure 5: Steady-state hydraulic head contours in the L-shaped aquifers with three different anisotropy ratios for $\kappa_1 = \kappa_2 = \kappa$.
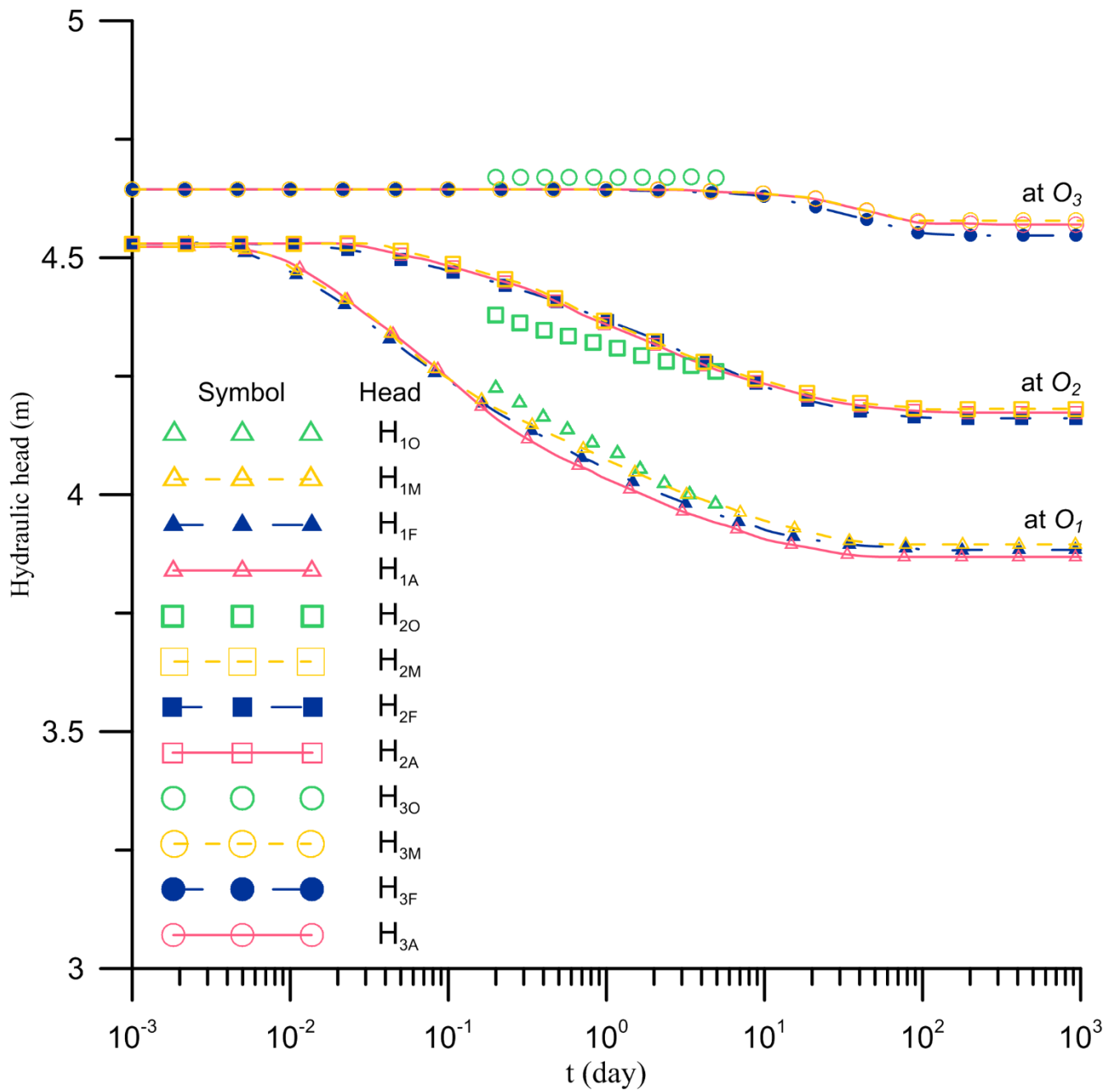
Figure 6: Temporal distributions of hydraulic head H_{io} observed at piezometer O_i and H_{iF} simulated by the FEM simulations both reported in Kihm et al. (2007) and H_{iA} and H_{iM} predicted by the present solution and MODFLOW, respectively, for $i = 1, 2, 3$.
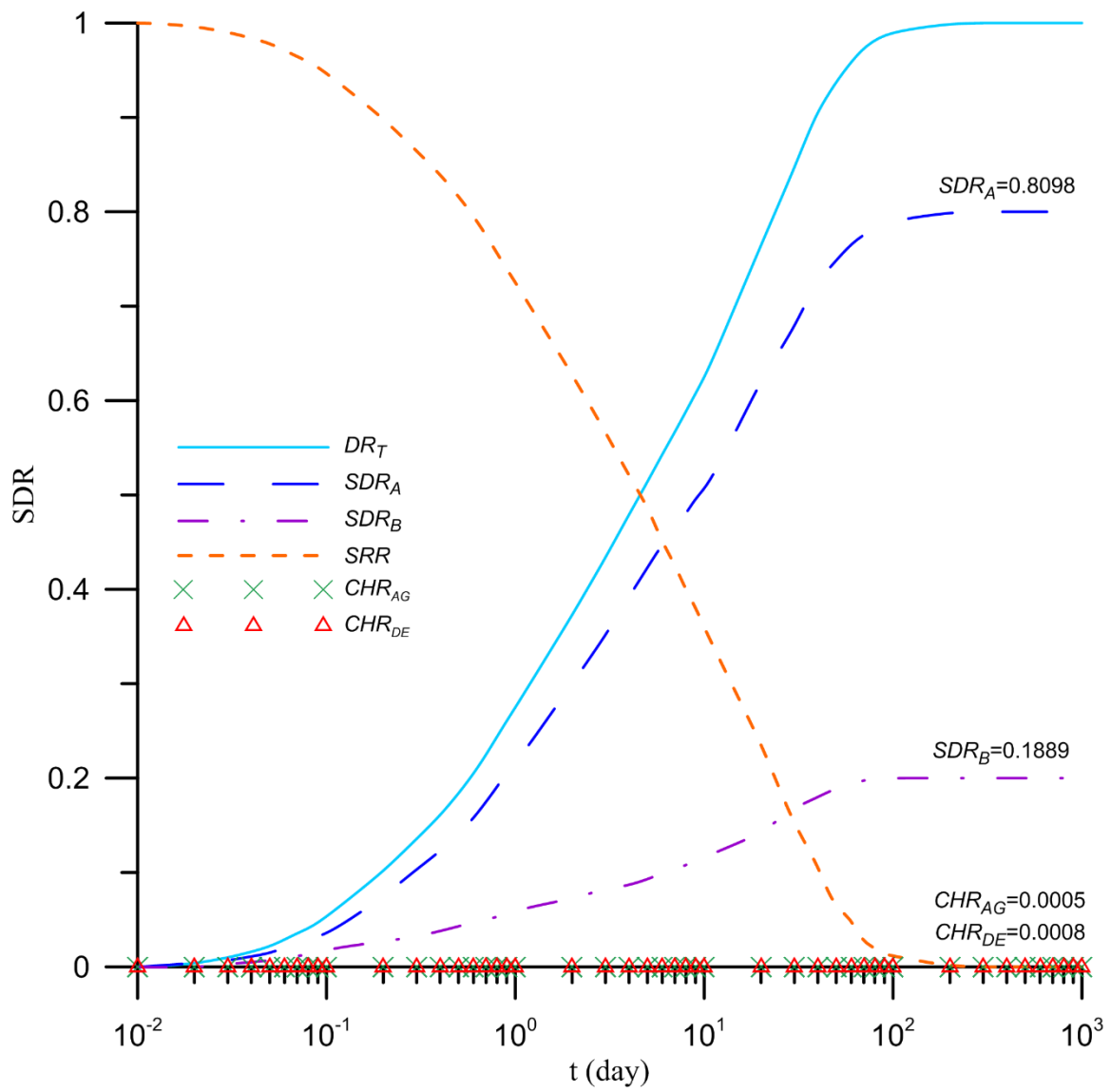
Figure 7: Temporal distributions of *SDRs*, *CHRs* and *SRR* due to pumping at *P_w*.